High-spin level structure of ^{35}S

S. Aydin,[1,2] M. Ionescu-Bujor,[3] F. Recchia,[2] S. M. Lenzi,[2] M. Bouhelal,[4] D. Bazzacco,[2] P. G. Bizzeti,[5] A. M. Bizzeti-Sona,[5] G. de Angelis,[6] I. Deloncle,[7] E. Farnea,[2,*] A. Gadea,[6,8] A. Gottardo,[2,6] F. Haas,[9] T. Huyuk,[8] H. Laftchiev,[10] S. Lunardi,[2] D. Mengoni,[2,11] R. Menegazzo,[2] C. Michelagnoli,[2] D. R. Napoli,[6] A. Poves,[12] E. Sahin,[6] P. P. Singh,[6] D. Tonev,[10] C. A. Ur,[2] and J. J. Valiente-Dobón[6]

[1]*Department of Physics, University of Aksaray, Aksaray, Turkey*
[2]*Dipartimento di Fisica e Astronomia dell'Università and INFN, Sezione di Padova, Padova, Italy*
[3]*Horia Hulubei National Institute of Physics and Nuclear Engineering, Bucharest, Romania*
[4]*Laboratoire de Physique Appliquée et Théorique, Université de Tebessa, Algeria*
[5]*Dipartimento di Fisica dell' Universitá and INFN Sezione di Firenze, Firenze, Italy*
[6]*INFN-Laboratori Nazionali di Legnaro, I-46020 Legnaro, Italy*
[7]*IPNO, IN2P3/CNRS et Université Paris-Sud, Orsay, France*
[8]*Instituto de Física Corpuscular, CSIC-Universidad de Valencia, Valencia, Spain*
[9]*IPHC, IN2P3/CNRS, Université de Strasbourg, Strasbourg, France*
[10]*Institute for Nuclear Research and Nuclear Energy, BAS, Sofia, Bulgaria*
[11]*University of the West of Scotland, Paisley, United Kingdom*
[12]*Departamento de Física Teórica e IFT-UAM/CSIC, Universidad Autónoma de Madrid, Madrid, Spain*

(Received 20 November 2013; published 13 January 2014)

The nucleus ^{35}S has been studied by in-beam γ-ray spectroscopy using the ^{24}Mg(^{14}N,3p) fusion-evaporation reaction at $E_{\rm lab} = 40$ MeV. A level scheme extended up to $J^\pi = 17/2^+$ at 8023 keV and $J^\pi = 13/2^-$ at 6352 keV has been established. Lifetimes of six excited states have been determined by applying the Doppler shift attenuation method. The experimental data have been compared with the results of large-scale shell model calculations performed using different effective interactions and model spaces allowing particle-hole excitations across the $N = Z = 20$ shell gap.

DOI: 10.1103/PhysRevC.89.014310 PACS number(s): 21.10.Re, 23.20.Lv, 21.60.Cs, 21.10.Hw

I. INTRODUCTION

The structure of the sd-shell nuclei is subject of a renewed interest in recent years. The use of heavy-ion beams in conjunction with large γ-ray and particle-detector arrays allowed to extend the experimental information, limited previously mainly to low- and medium-spin states [1], in the range of high spins [2–16]. In these nuclei, the low-spin structure of positive parity states at not too high energy can be well reproduced by shell model calculations using the universal sd-shell interaction (USD) introduced by Wildenthal [17]. At high spin and also higher energy, the excitation of particles from the sd shell to the fp shell have to be taken into account, and the experimental data serve as a testing ground of recently proposed effective interactions [18–22]. Interesting results, pointing to a complex structure of coexisting spherical, deformed, and superdeformed states, were reported in ^{36}Ar [2], ^{38}Ar [4], ^{40}Ca [5], and very recently in ^{35}Cl [16], and described by large scale shell model calculations involving multiparticle-multihole intruder excitations from the sd to the fp shell [23].

Excited states of ^{35}S have been studied previously in ^{35}P β^- decay [24], ^{34}S(n,γ) [25], ^{34}S($d,p\gamma$) [26], ^{37}Cl(p,^{3}He) [27] ^{37}Cl($d,\alpha\gamma$) [28], and a pn transfer from a ^{37}Cl beam to a ^{160}Gd target [29]. Only states of low spin, $J \leqslant 7/2$, have been reported on this nucleus [30]. The present work is devoted to the investigation of the high-spin states in ^{35}S by in-beam γ-ray spectroscopy. The experimental procedure and the new results are presented in Sec. II. A comparison of the experimental data with the predictions of large-scale shell-model calculations is given in Sec. III. The results of the work are summarized in Sec. IV.

II. EXPERIMENTAL PROCEDURE AND RESULTS

High-spin states of ^{35}S have been populated via the fusion-evaporation reaction ^{24}Mg(^{14}N,3p)^{35}S at 40 MeV bombarding energy. A ^{14}N beam delivered by the LNL XTU-Tandem accelerator impinged on the target with an average beam current of 5 pnA. The 99.7% isotopically enriched ^{24}Mg target, 1 mg/cm^2 thick, was evaporated on an 8 mg/cm^2 gold layer. The γ rays emitted in the reaction were detected using the 4π-GASP array [31] composed of 40 Compton-suppressed large volume high-purity Ge detectors arranged in seven rings at different angles with respect to the beam axis. Events were collected when at least two germanium detectors fired in coincidence.

The data were sorted into a symmetric γ-γ matrix and seven asymmetric matrices having the detectors at 34°, 60°, 72°, 90°, 108°, 120°, 146°, respectively, on the first axis, and all detectors on the second axis. The symmetric matrix has been used to study γ-γ coincidence relationships for the construction of the level scheme, while the asymmetric matrices were used to obtain information about the γ transition multipolarities. To this purpose, the efficiency-corrected γ-ray intensities, $I_\gamma(\theta)$, were derived from spectra gated on the axis with all the detectors. They are used to calculate the angular

*Deceased.

distribution ratio R_{ADO} defined as [32]: $R_{\mathrm{ADO}} = (I_\gamma(34^\circ) + I_\gamma(146^\circ))/2I_\gamma(90^\circ)$. In the present experimental conditions typical R_{ADO} values are 0.8 for pure dipole stretched transitions and 1.4 for quadrupole stretched or $\Delta J = 0$ pure dipole transitions. In the case of a quadrupole/dipole admixture, R_{ADO} depends on the value and sign of the mixing coefficient δ [33]. For the most intense transitions full angular distributions $W(\theta)$ could be also derived. They were fitted to the Legendre polynomial function $1 + A_2P_2[\cos(\theta)] + A_4P_4[\cos(\theta)]$, in order to determine the angular distribution coefficients $A_{2,4}$.

Due to the presence of Doppler-broadened shapes, relative γ intensities were obtained by integrating on the broaden lines in spectra created from the asymmetric matrices. To minimize the angular distribution effects, matrices at 60° and 120° were used. The asymmetric matrices have been also used for lifetime determinations.

A. Level scheme of ^{35}S

Prior to our study only low-spin states with $J \leqslant 7/2$ have been reported in ^{35}S [30]. The ground state has $J = 3/2^+$ and the lowest-lying positive-parity states, at excitation energy of 1572 and 2717 keV, have spins $1/2^+$ and $5/2^+$, respectively. The lowest-lying negative-parity state at 1991 keV is a $7/2^-$ isomer with a half-life of 1.02(5) ns, and a $3/2^-$ state is known at 2348 keV excitation energy.

In the present work the level scheme of ^{35}S has been considerably extended to larger spins and excitation energies with respect to previous studies. Nine new states, seven of positive parity and two of negative parity, and 28 new γ-ray transitions, have been added. Moreover, firm spin-parity was assigned to four previously known levels. The deduced level scheme is shown in Fig. 1. The level energies and the assigned spins and parities, as well as the transition energies, R_{ADO} values, relative intensities, and multipolarities are given in Table I.

The level scheme has been constructed on the basis of coincidence relationships in spectra created with appropriate gates on the symmetric γ-γ matrix. Figure 2(a) illustrates the coincidence spectrum obtained by gating on the 1991 keV transition de-exciting the $7/2^-$ state in ^{35}S. An interesting feature revealed in this spectrum was that the γ rays presented

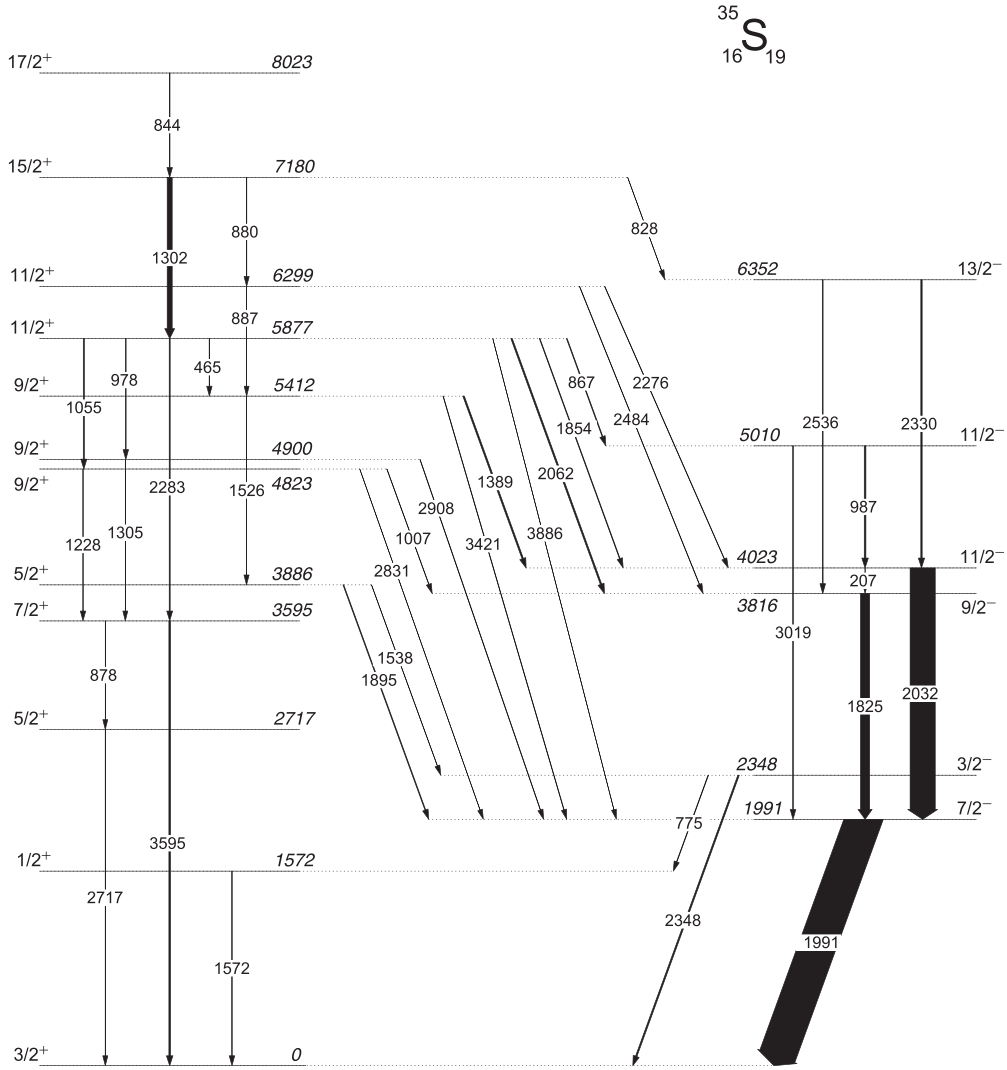

FIG. 1. Level scheme of ^{35}S established in the present work.

TABLE I. Initial state energies, spins, and parities for initial and final states and transition energies in ^{35}S, as well as $R_{\rm ADO}$ values, relative intensities and multipolarities. Previously known states are marked with a star (⋆).

E_i(keV)	J_i^π	J_f^π	E_γ(keV)	$I_\gamma^{\rm rel}$	$R_{\rm ADO}$	Multipolarity
1572.4⋆	$1/2^+$	$3/2^+$	1572.4(3)	14(4)	0.88(10)	$M1$
1991.3⋆	$7/2^-$	$3/2^+$	1991.3(2)	1000(57)	1.45(15)	$M2+E3$
2347.8⋆	$3/2^-$	$1/2^+$	775.4(4)	14(2)	0.68(14)	$E1$
		$3/2^+$	2347.8(3)	38(3)		
2717.0⋆	$5/2^+$	$3/2^+$	2717.0(4)	5(3)		
3594.7⋆[a]	$7/2^+$	$5/2^+$	877.6(5)	4(1)		
		$3/2^+$	3594.7(7)	43(4)	1.36(16)	$E2$
3815.9⋆[a]	$9/2^-$	$7/2^-$	1824.6(2)	249(15)	1.58(5)	$M1+E2$
3886.2⋆[a]	$5/2^+$	$3/2^-$	1538.4(8)	5(2)		
		$7/2^-$	1894.9(4)	21(3)	0.69(10)	$E1$
4023.0⋆[a]	$11/2^-$	$9/2^-$	207.0(5)	4(2)		
		$7/2^-$	2031.8(3)	677(38)	1.41(6)	$E2$
4822.7	$9/2^+$	$9/2^-$	1006.8(2)	8(1)	1.37(11)	$E1$
		$7/2^+$	1228.1(3)	11(1)	0.78(9)	$M1$
		$7/2^-$	2831.4(9)	4(1)		
4899.6	$9/2^+$	$7/2^+$	1304.8(12)	0.6(2)		
		$7/2^-$	2908.3(5)	11(2)	0.74(14)	$E1$
5009.7	$11/2^-$	$11/2^-$	986.9(3)	44(2)	1.30(13)	$M1$
		$7/2^-$	3018.5(7)	19(2)	1.35(34)	$E2$
5411.9	$9/2^+$	$11/2^-$	1389.0(4)	39(4)	0.79(11)	$E1$
		$5/2^+$	1525.7(8)	6(1)		
		$7/2^-$	3420.6(9)	11(1)		
5877.3	$11/2^+$	$9/2^+$	465.3(3)	12(1)	0.71(9)	$M1$
		$11/2^-$	867.3(3)	19(1)	1.36(20)	$E1$
		$9/2^+$	977.8(3)	16(1)	1.43(16)	$M1+E2$
		$9/2^+$	1054.5(3)	30(2)	0.72(11)	$M1$
		$11/2^-$	1854.4(4)	17(1)		
		$9/2^-$	2061.5(3)	38(2)	0.65(9)	$E1$
		$7/2^+$	2282.9(4)	26(1)		
		$7/2^-$	3886.0(13)	3(1)		
6299.0	$11/2^+$	$9/2^+$	887.0(7)	4(1)	0.6(3)	$M1$
		$11/2^-$	2275.9(6)	10(2)		
		$9/2^-$	2483.6(8)	9(2)		
6352.1	$13/2^-$	$11/2^-$	2329.5(9)	36(7)	0.8(3)	$M1$
		$9/2^-$	2535.8(11)	18(2)	1.5(5)	$E2$
7179.5	$15/2^+$	$13/2^-$	827.8(6)	3(1)		
		$11/2^+$	880.2(4)	8(1)		
		$11/2^+$	1302.2(2)	135(8)	1.40(5)	$E2$
8023.4	$17/2^+$	$15/2^+$	843.9(8)	16(2)	0.8(3)	$M1$

[a]Spin-parity of previously known state is assigned in this work.

unshifted components that were observed as narrow peaks. This was due to the fact that the state located at 7180-keV excitation energy, that populates in its decay all lower-lying states, has a relatively long half-life, of about 3 ps (see next subsection) and therefore the decay takes place mostly at rest in the thick target. A coincidence spectrum gated by the 1302-keV γ ray de-exciting the 7180-keV state is shown in Fig. 2(b). Note that transitions of 844, 2330, and 2536 keV, de-exciting the highest-lying states of positive and negative parity, respectively, (Fig. 1) show large Doppler broadening (see below) and therefore are not seen in the spectra obtained from the symmetric γ-γ matrix of Fig. 2.

The angular distributions of the 1302-, 1825-, and 2032-keV intense transitions and the best-fit values of the $A_{2,4}$ coefficients, are illustrated in Fig. 3. A pure quadrupole multipolarity was assigned to the 1302- and 2032-keV transitions, while for the 1825-keV transition an $M1+E2$ mixed multipolarity was established, with a mixing ratio $\delta(E2/M1) = 0.55(9)$.

Spins and parities for the new levels have been assigned on the basis of transition multipolarities deduced from measured $R_{\rm ADO}$ values, angular distribution analysis, and/or lifetime considerations. The common assumption, for fusion-evaporation reactions, of assigning increasing angular momentum when increasing the excitation energy of the states, has been applied. The stretched quadrupole transitions were assigned as $E2$ on the basis of lifetime measurements (see next subsection), as the $M2$ multipolarity would correspond to transition strengths, much larger than the upper limit of 3 W.u. expected for this mass region [34]. For all new states there is at least one transition with measured $R_{\rm ADO}$ and deduced multipolarity. The spin and parity assignment was further checked to be consistent with the multipolarities for all the other feeding and de-exciting transitions.

The most intense transition in the level scheme is the known 1991 keV from the $7/2^-$ state to the $3/2^+$ ground state. Its deduced $R_{\rm ADO}$ value is in accordance with the assigned $M2$ multipolarity. The $3/2^-$ state known at 2348-keV excitation energy was relatively weakly populated. The ADO ratio could be determined for the 775-keV de-exciting transition toward the $1/2^+$ state and is in accordance with the assigned $E1$ multipolarity.

The 1825- and 2032-keV transitions in coincidence with the 1991-keV line were previously observed as de-exciting states at 3816 and 4023 keV, respectively, however spins were not firmly assigned [30]. In our study the multipolarities of these transitions have been established through the measurement of their angular distributions (see Fig. 3), leading to spin-parity $9/2^-$ and $11/2^-$ for the 3816- and 4023-keV levels, respectively. The 4023-keV state decays with a newly observed 207-keV transition to the 3816-keV level.

A new state was found at 5010 keV excitation energy and assigned as the second $11/2^-$ state, based on its observed decays, namely the 3019-keV $E2$ and 987-keV $M1$ transitions to the yrast $7/2^-$ 1991 keV and $11/2^-$ 4023 keV states, respectively.

The highest negative-parity spin identified in the present work was $13/2^-$ assigned to the new state at 6352 keV. This state decays through the 2330- and 2536-keV γ transitions of multipolarities $M1$ and $E2$, to the $11/2^-$ and $9/2^-$ states, respectively. Note that these γ lines have large Doppler shifts and no stopped component and therefore could not be seen in spectra from the symmetric γ-γ matrix. They were observed in spectra obtained from the asymmetric matrix corresponding to the detectors placed at 90°.

On the positive-parity side the known $1/2^+$ and $5/2^+$ lowest-lying states, de-excited by the 1572- and 2717-keV γ rays, respectively, were relatively weakly populated in the present work. The $R_{\rm ADO}$ value determined for the 1572-keV transition to the ground state is in agreement with the assigned

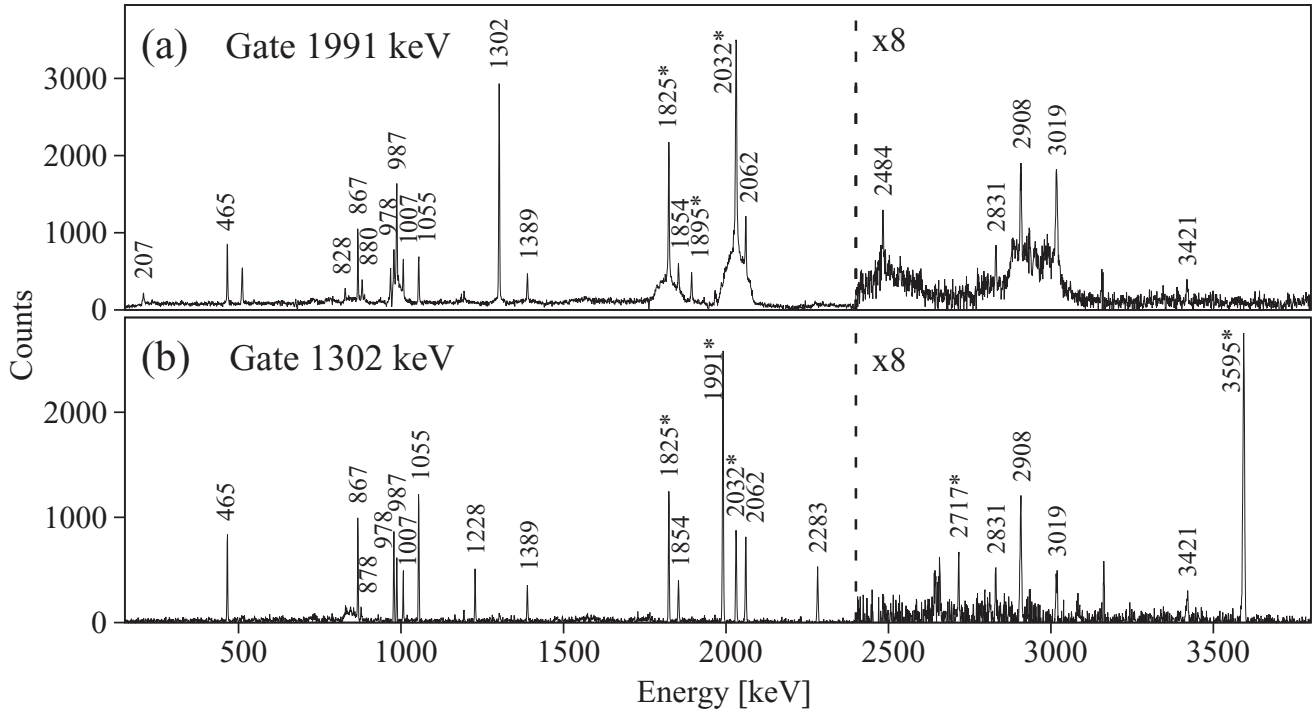

FIG. 2. Background-subtracted coincidence spectra obtained from the symmetric γ-γ matrix. The γ rays in ^{35}S are labeled by the energy. Previously known γ rays are marked with a star ($\star$). Unmarked peaks are due to random coincidences resulting from the large background.

$M1$ character. The 3595-keV state, known from previous studies but without spin assignment [30], has been identified as the yrast $7/2^+$ state, on the basis of the $E2$ multipolarity established for the 3595-keV de-exciting transition to the $3/2^+$ ground state.

A new state identified at 5877 keV was assigned the yrast $11/2^+$ state, as it is feeding the $7/2^+$ 3595-keV state by the $E2$ 2283-keV transition. The $11/2^+$ state populates by the $M1$ transitions of 1055, 978, and 465 keV new levels at 4823, 4900, and 5412 keV, respectively, assigned as $9/2^+$ states. Spin-parity $5/2^+$ was given to the previously known state at 3886-keV excitation energy, that is decaying by the $E1$ 1895-keV transition to the $7/2^-$ state and by the 1538-keV transition to the 2348-keV state. The assignment is supported by the fact that the state is populated by the 1526-keV γ ray from the $9/2^+$ state at 5412 keV. The second $11/2^+$ state is located at 6299 keV and decays through the 887-keV $M1$ transition to the $9/2^+$ level at 5412 keV.

The yrast $15/2^+$ state was identified at 7180 keV, based on the observation of the $E2$ 1302-keV intense transition linking it to the first $11/2^+$ state. The highest spin observed in our experiment, $17/2^+$, was assigned to the state located at 8023 keV, de-excited through the 844-keV transition of multipolarity $M1$ to the $15/2^+$ level. As in the case of the γ transitions de-exciting the $13/2^-$ state, the 844-keV transition has large Doppler broadening and could not be seen in spectra from the symmetric γ-γ matrix. This γ line was observed in spectra obtained from the asymmetric matrix corresponding to the detectors placed at 90°. No state with spin $13/2^+$ could be identified in the present work, most probably because it is less populated. This could indicate that the $13/2^+$ state is located very near the $15/2^+$ state, eventually above it, and the feeding from higher spins states go preferentially toward this yrast $15/2^+$ state.

A characteristics of the level scheme is that all positive-parity states above the yrast $7/2^+$ state have significant decays by $E1$ transitions to the negative parity states, as seen in Fig. 1 and Table I. This behavior could indicate a change of structure that involves nucleon excitations in the negative-parity orbitals.

B. Lifetime measurements

The lifetimes of the medium- and high-spin states in ^{35}S have been investigated by the Doppler shift attenuation method (DSAM). The analysis has been performed using the LINE-SHAPE code [35], modified in order to allow, for each level, side populations from two independent levels. This was particularly important in the present case where the lower-lying levels have a fraction of their population coming from a longer lived state. The slowing down history of ^{35}S recoils in the target and backing was simulated using Monte Carlo techniques and a statistical distribution was created for the projection of the recoil velocity with respect to the direction of the detected γ ray. Moreover, the kinematic effects of the nucleon evaporation were included, as well as the finite solid angle of the detectors. For the description of the electronic and nuclear scattering the Ziegler [36,37] stopping powers have been adopted. To estimate the systematic error introduced by the stopping powers, several intense transitions have been also analyzed using the Northcliffe-Schilling parametrization [38] corrected for atomic shell effects [39]. The lifetimes derived using the two parametrizations were found consistent within 10%. We assigned therefore a conservative systematic uncertainty of 12% due to the stopping power calculation.

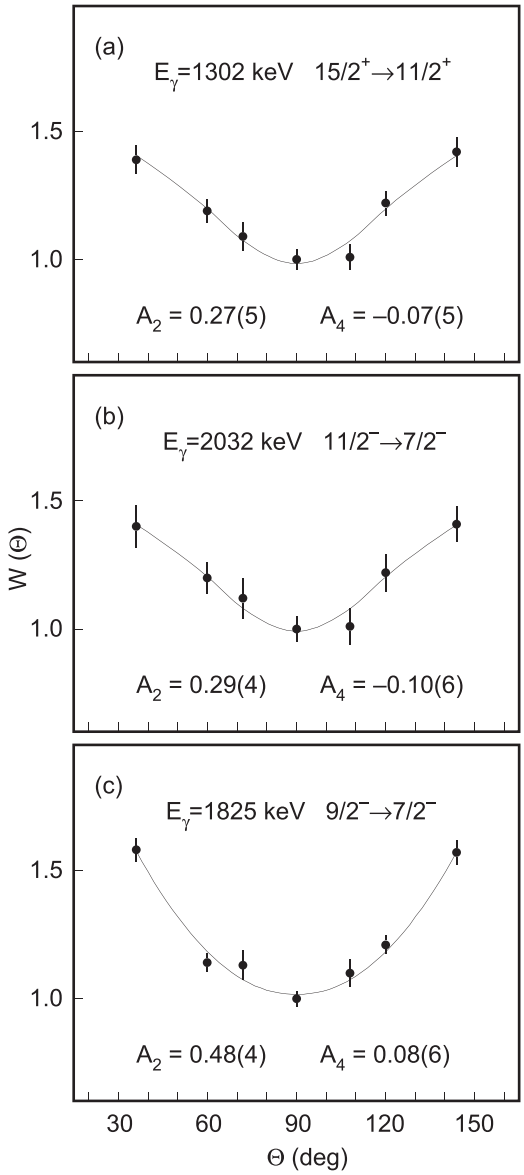

FIG. 3. Angular distribution of the 1302-, 1825-, and 2032-keV transitions de-exciting the states at 7180, 3816, and 4023 keV, respectively, in ^{35}S. The fitted values of the angular distribution coefficients are reported in the figure.

The analysis was done in spectra created from the asymmetric γ-γ matrices using a narrow gate on the intense 1991-keV γ line emitted from stopped nuclei. For each level the intensity balance of feeding and decaying transitions was calculated using the γ intensities of Table I, allowing to establish the amount of the fast side-feeding from unobserved transitions. Lifetimes have been derived for the $9/2^-$, $11/2^-_1$, $11/2^-_2$, and $13/2^-$ negative-parity states and for the $15/2^+$ and $17/2^+$ positive-parity states. The states with positive-parity medium spin values, from $7/2^+$ to $11/2^+$, were weakly populated, a fact that prevented a reliable DSAM analysis of the de-exciting transitions. Examples of experimental lineshapes and the corresponding fits are illustrated in Fig. 4. As seen in Fig. 4, the 1302 keV transition de-exciting the $15/2^+$ state of 7180 keV excitation energy has a dominant stopped component and presents small angle-dependent tails, corresponding to a rather long lifetime, $T_{1/2} = 3.1(12)$ ps. Shorter lifetimes, in the subpicosecond range, were derived for the other investigated states. The results of lifetime measurements are collected in Table II.

III. COMPARISON WITH SHELL-MODEL PREDICTIONS

To interpret the observed properties of ^{35}S, we have performed shell model calculations using different interactions and model spaces. The calculations have been done with the shell model code ANTOINE [40].

In a first stage, positive parity states have been calculated in the *sd* valence space using the USD effective interaction [17]. The comparison between the experimental states and the calculated ones is shown in Fig. 5. We note a very good agreement between experimental and calculated states up to the spin $7/2^+$. The higher spin states are predicted at much higher energies than those observed experimentally. This indicates that the restricted *sd* model space is not good enough for states with spin higher than $7/2^+$, for which particle-hole excitations to the *fp* shell contribute to the wave functions.

A second calculation was performed by using a new interaction developed by Bouhelal *et al.* [22], the PSDPF interaction. This interaction considers the full *psdpf* model space with a ^{4}He core. Negative parity states of $1\hbar w$ nature can be obtained by allowing one nucleon jump between major shells. The results for positive and negative parity states are reported in Figs. 5 and 6, respectively. The results for the positive parity states are similar to those obtained with the USD interaction. A good description is provided up to the $7/2^+$ state, while the higher-lying states are predicted too high in excitation energy. Note that the energy of the third $5/2^+$ state is also overestimated by the calculations, indicating that at least $2p$-$2h$ excitations toward the *fp* shell could be present. This is in accordance with the observed decay of the state toward negative-parity states. A remarkable good description is provided for all observed negative-parity states, what indicates that up to spin $13/2^-$ the states contain only one excitation in the *fp* orbitals.

To allow more than one particle-hole excitation to the *fp* shell, we have adopted the model space spanned by the $s_{1/2}$,$d_{3/2}$, $f_{7/2}$, and $p_{3/2}$ orbits. The interaction in this model space is the *sdfp* interaction [21]. The results are also shown in Figs. 5 and 6. The $5/2^+$ states are predicted higher compared to the observed states. This is mainly due to the fact that in these calculations the $d_{5/2}$ orbital is kept closed, while the role of this orbital seems important, as indicated by the USD and PSDPF calculations. For all positive-parity states with $J^\pi \geqslant 9/2^+$ the calculations predict a wave function configuration with two neutrons promoted in the *fp* shell. This is consistent with the decay pattern of these states showing large branchings toward the negative-parity states. In the calculations the first $11/2^+$ state is predicted below the $9/2^+$ states, in disagreement with the experimental data. Note that the yrast $13/2^+$ state is calculated above the $15/2^+$ state; this is in accordance with the fact the $13/2^+$ state is not observed experimentally, being very weakly populated. The *sdfp* negative-parity states are also in

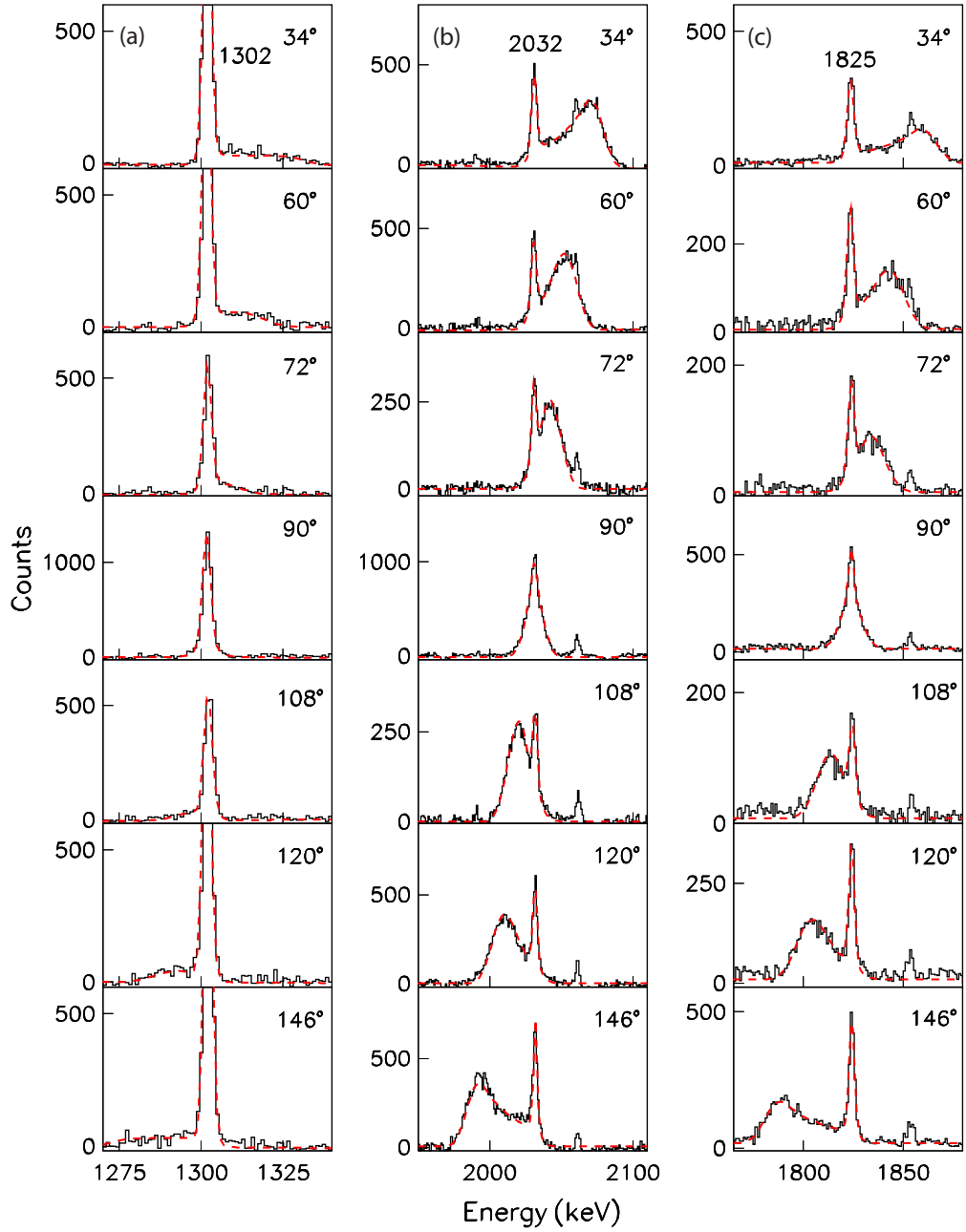

FIG. 4. (Color online) Experimental and calculated lineshapes for the 1302-, 2032-, and 1825-keV transitions de-exciting the states at 7180, 4023, and 3816 keV, respectively, in ^{35}S. The fitted DSAM spectra are shown in red dashed line.

a good accordance with the experimental states, as seen in Fig. 6, at least till $J^\pi = 11/2^-$.

The *sdfp* effective interaction was recently used in the description of odd-mass ^{37}Cl [11] and odd-odd ^{36}Cl [14] nuclei. In these references it was pointed out that a better reproduction of the experimental findings was obtained with an increase by 500 keV in the single-particle energy of the $f_{7/2}$ orbital. We have therefore performed shell-model calculations for ^{35}S using this modified interaction, however the description of the observed experimental data was not improved in this case.

TABLE II. Half-lives determined in the present work for excited states in ^{35}S.

E_x (keV)	J^π	$T_{1/2}$ (ps)
3816	$9/2^-$	0.28(3)
4023	$11/2^-$	0.32(3)
5010	$11/2^-$	0.45(8)
6352	$13/2^-$	0.05(1)
7180	$15/2^+$	3.1(12)
8023	$17/2^+$	0.15(4)

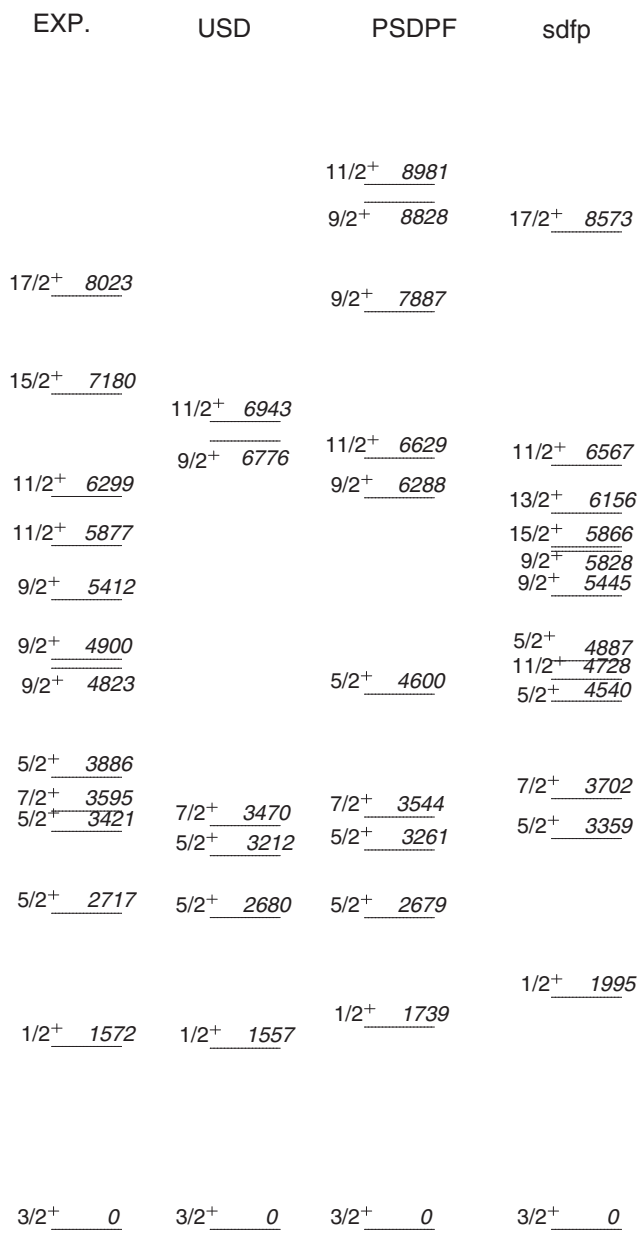

FIG. 5. Experimental positive-parity states of ^{35}S compared with shell-model calculations using the code ANTOINE with different model spaces and interactions. The second $5/2^+$ state, not observed in the present experiment, was taken from [30].

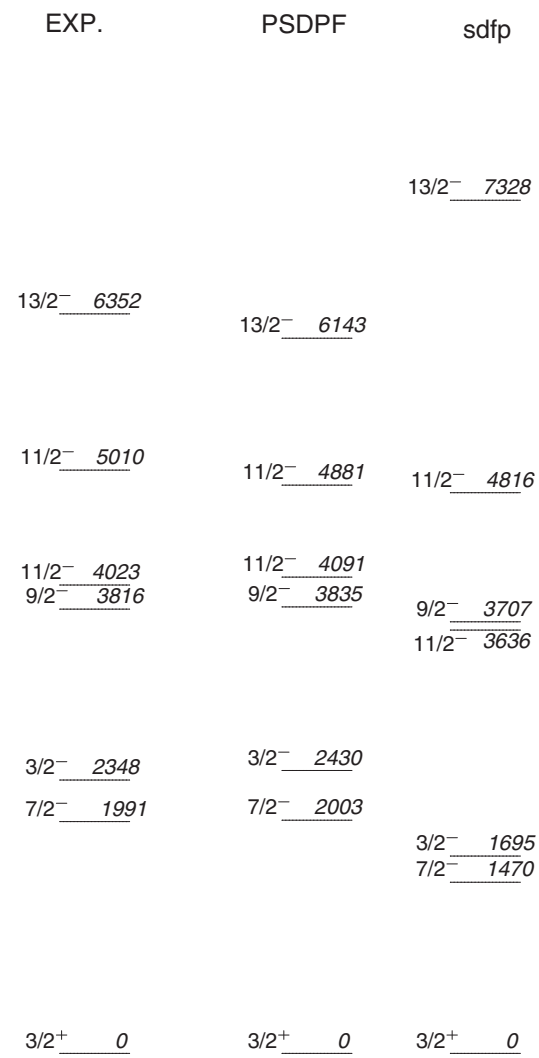

FIG. 6. Negative parity states of ^{35}S observed in the present experiment compared with shell-model calculations using the code ANTOINE with different model spaces and interactions.

Finally a new interaction, SDPF-U-MIX has been recently introduced involving the *sd* and *fp* main shells for protons and neutrons [41]. These calculations predict the $0p$-$0h$ $9/2^+$ and $11/2^+$ states at 6.28 and 6.44 keV, respectively, consistent with the PSDPF calculations. On the other hand, the $2p$-$2h$ yrast $9/2^+$, $11/2^+$, $13/2^+$, $15/2^+$, and $17/2^+$ states are expected at 5.52, 5.99, 6.82, 6.73, and 8.53 keV, respectively, in better agreement with the experimental data.

The structure of the level scheme can therefore be interpreted in the light of the wave-function configurations in the following way. The positive-parity states up to $7/2^+$ involve only excitations within the *sd* shell. Positive-parity states with $J \geqslant 9/2$ involve two neutron excitations into the *fp* shell. Some states present particular characteristics, as for example the $15/2^+$ state that corresponds to the maximum angular momentum that can be obtained with the excitation of two neutrons without breaking a proton pair. It is interesting to point out that in Ref. [42] a state identified in ^{36}S at 6690 keV excitation energy, with a lifetime longer than 1 ps, was tentatively assigned as the yrast 6^+ state and described by a stretched configuration with two neutrons in the $f_{7/2}$ orbit. The $15/2^+$ state at 7180 keV in ^{35}S could be thus the stretched configuration 6^+ in ^{36}S coupled to a neutron hole in the $d_{3/2}$ orbital. On the negative parity side, the $7/2^-$ state corresponds to the excitation of one neutron into the $f_{7/2}$ shell, while the first $11/2^-$ state has the maximum spin reachable with such a neutron excitation without breaking a proton pair. These states are characterized in the decay scheme by strong γ-ray de-excitation transitions.

Using the measured half-lives (from Ref. [30] and this work) and the branching ratios (BR) derived from the presently

TABLE III. Experimental reduced transition probabilities B(M1) and B(E2) in ^{35}S compared to shell model calculations performed with the code ANTOINE using the USD, PSDPF, and $sdfp$ residual interactions (see text for details).

$E_{\rm lev}^{\rm exp}$	$T_{1/2}^{\rm exp}$	J_i^π	J_f^π	$E_\gamma^{\rm exp}$	BR[b]	$B(\mathrm{M1})(\mu_N^2)$				$B(E2)(e^2\mathrm{fm}^4)$			
(keV)	(ps)			(keV)	%	exp	USD	PSDPF	$sdfp$	exp	USD	PSDPF	$sdfp$
1572	2.3(4)[a]	$1/2_1^+$	$3/2_1^+$	1572	100	0.004(1)	0.024	0.020	0.002				
2717	0.069(24)[a]	$5/2_1^+$	$3/2_1^+$	2717	100	0.028(10)	0.032	0.038	0.000				
7180	3.1(1.2)[b]	$15/2_1^+$	$11/2_1^+$	1302	93(2)					45(17)	7	9	31
8023	0.15(4)[b]	$17/2_1^+$	$15/2_1^+$	844	100	0.44(12)	0.72	1.134	0.002				
3816	0.28(3)[b]	$9/2_1^-$	$7/2_1^-$	1825	100	0.018(4)		0.019	0.008	23(8)		48	5
4023	0.32(3)[b]	$11/2_1^-$	$7/2_1^-$	2032	99(1)					51(5)		48	14
5010	0.45(8)[b]	$11/2_2^-$	$11/2_1^-$	987	70(3)	0.064(12)		0.040	0.020				
			$7/2_1^-$	3019	30(3)					1.5(3)		1.3	21
6352	0.05(1)[b]	$13/2_1^-$	$11/2_1^-$	2330	66(10)	0.04(1)		0.037	0.001				
			$9/2_1^-$	2536	34(5)					37(9)		26	18

[a]Reference [30].
[b]Present study.

determined γ-ray intensities, the experimental $B(M1)$ and $B(E2)$ reduced transition probabilities have been obtained. They are presented in Table III together with the PSDPF and $sdfp$ shell-model calculations. For the 1825 keV $M1+E2$ mixed transition, both $B(M1)$ and $B(E2)$ experimental values have been derived, using the δ value deduced on the basis of angular distribution analysis. In USD and $sdfp$ calculations, effective g factors have been used, with values $g_{\nu s}^{\rm eff} = -2.869$, $g_{\nu \ell}^{\rm eff} = -0.1$, $g_{\pi s}^{\rm eff} = 4.189$, $g_{\pi \ell}^{\rm eff} = 1.1$, while the $B(E2)$ have been obtained using the effective electric charges $e_\nu^{\rm eff} = 0.46e$ and $e_\pi^{\rm eff} = 1.31e$. The PSDPF calculations were performed using parameters fitted using USDA and USDB through new experimental values given in Ref. [43]. The values $g_{\nu s}^{\rm eff} = -3.55$, $g_{\nu \ell}^{\rm eff} = -0.09$, $g_{\pi s}^{\rm eff} = 5.150$, $g_{\pi \ell}^{\rm eff} = 1.159$, were adopted for the $B(M1)$ and $B(M2)$ calculation, while effective charges of $0.45e$ and $1.36e$ for neutron and proton, respectively, were used for the $B(E2)$ and $B(E3)$ determination.

We note a remarkable good agreement between the experimental $B(M1)$ and $B(E2)$ reduced transition probabilities and the values calculated using the PSDPF interaction. This gives further support for the validity of this new effective interaction in the description of low- and medium spin states of sd nuclei. The only experimental values not well reproduced are those for the decay of the $15/2^+$ and $17/2^+$ high-spin positive-parity states, that are involving two neutron excitations in the fp shell, not included in the PSDPF interaction.

The predictions of the $sdfp$ calculations are in moderate agreement with experimental $B(M1)$ and $B(E2)$ values, as seen in Table III. Note that the $B(E2)$ value of the $15/2_1^+ \rightarrow 11/2_1^+$ transition is well reproduced by the $sdfp$ calculations, in which the involved states are both described by the promotion of two nucleons into the fp shell.

Shell model calculations with the PSDPF residual interaction were also performed to derive reduced transition probabilities for parity changing $E1$, $M2$, and $E3$ transitions de-exciting the lowest-lying $7/2^-$ and $3/2^-$ states in ^{35}S. The lifetimes, branching ratios and mixing ratios used in deriving the experimental reduced transition probabilities were taken from Ref. [30]. The theoretical $B(E1)$ have been obtained using effective electric charges of $-eZ/A$ and eN/A for the neutron and proton, respectively. The comparison between the experimental and calculated values is shown in Table IV. We note disagreement in the case of the 2348-keV $E1+M2$ mixed transition, where the theoretical transition probabilities are underestimating the experimental ones. On the other hand the $B(M2)$ and $B(E3)$ values of the 1991 keV transition, and the $B(E1)$ value of the 775 keV transition, are well reproduced by the shell-model calculations.

IV. SUMMARY

A detailed spectroscopic study of the nucleus ^{35}S, extended at high spin, has been done for the first time. Nine new states,

TABLE IV. Experimental reduced transition probabilities $B(E1)$, $B(M2)$, and $B(E3)$ in ^{35}S compared to shell model calculations performed with the code ANTOINE using the PSDPF residual interaction (see text for details).

$E_{\rm lev}^{\rm exp}$	$T_{1/2}^{\rm exp}$	J_i^π	J_f^π	$E_\gamma^{\rm exp}$	BR[a]	$B(E1)(e^2\mathrm{fm}^2)$		$B(M2)(\mu_N^2\mathrm{fm}^2)$		$B(E3)(e^2\mathrm{fm}^6)$	
(keV)	(ps)			(keV)	%	exp	PSDPF	exp	PSDPF	exp	PSDPF
1991	1020(50)[a]	$7/2_1^-$	$3/2_1^+$	1991	100			1.6(5)	2.11	115(86)	119
2348	0.81(14)[a]	$3/2_1^-$	$1/2_1^+$	775	27(1)	$32(6) \times 10^{-5}$	54×10^{-5}				
			$3/2_1^+$	2348	73(1)	$31(6) \times 10^{-6}$	10×10^{-7}	45(18)	0.0044		

[a]Reference [30].

seven of positive parity and two of negative parity, and 28 new γ-ray transitions, have been added. Moreover, firm spin-parity was assigned to four previously known levels. Lifetimes have been determined for six states by applying the Doppler shift attenuation method. The data were compared to large scale shell model calculations using different effective interactions, which constitutes a benchmark and a very stringent test to these interactions that take into account excitations between two main shells. From this comparison it has been possible to identify the dominant configuration of both positive- and negative-parity states of low and medium spin.

ACKNOWLEDGMENTS

This work was carried out at the INFN Laboratori Nazionali di Legnaro (LNL), Italy. Authors are thankful to the XTU Tandem staff of LNL for delivering good quality beam.

[1] P. M. Endt, Nucl. Phys. A **521**, 1 (1990); **633**, 1 (1998), and references therein.
[2] C. E. Svensson *et al.*, Phys. Rev. Lett. **85**, 2693 (2000).
[3] C. E. Svensson *et al.*, Phys. Rev. C **63**, 061301(R) (2001).
[4] D. Rudolph *et al.*, Phys. Rev. C **65**, 034305 (2002).
[5] E. Ideguchi *et al.*, Phys. Rev. Lett. **87**, 222501 (2001).
[6] P. Mason *et al.*, Phys. Rev. C **71**, 014316 (2005).
[7] M. Ionescu-Bujor *et al.*, Phys. Rev. C **73**, 024310 (2006).
[8] F. Della Vedova *et al.*, Phys. Rev. C **75**, 034317 (2007).
[9] R. Kshetri *et al.*, Nucl. Phys. A **781**, 277 (2007).
[10] P. C. Bender *et al.*, Phys. Rev. C **80**, 014302 (2009).
[11] M. Ionescu-Bujor *et al.*, Phys. Rev. C **80**, 034314 (2009).
[12] R. Chakrabarti *et al.*, Phys. Rev. C **84**, 054325 (2011).
[13] P. J. R. Mason *et al.*, Phys. Rev. C **85**, 064303 (2012).
[14] S. Aydin *et al.*, Phys. Rev. C **86**, 024320 (2012).
[15] S. Szilner *et al.*, Phys. Rev. C **87**, 054322 (2013).
[16] A. Bisoi *et al.*, Phys. Rev. C **88**, 034303 (2013).
[17] B. H. Wildenthal, Prog. Part. Nucl. Phys. **11**, 5 (1984).
[18] E. K. Warburton, J. A. Becker, and B. A. Brown, Phys. Rev. C **41**, 1147 (1990).
[19] Y. Utsuno, T. Otsuka, T. Mizusaki, and M. Honma, Phys. Rev. C **60**, 054315 (1999).
[20] Y. Utsuno, T. Otsuka, T. Glasmacher, T. Mizusaki, and M. Honma, Phys. Rev. C **70**, 044307 (2004).
[21] E. Caurier, K. Langanke, G. Martinez-Pinedo, F. Nowacki, and P. Vogel, Phys. Lett. B **522**, 240 (2001).
[22] M. Bouhelal, F. Haas, E. Caurier, F. Nowacki, and A. Bouldjedri, Nucl. Phys. A **864**, 113 (2011).
[23] E. Caurier, F. Nowacki, and A. Poves, Phys. Rev. Lett. **95**, 042502 (2005).
[24] E. K. Warburton, D. E. Alburger, J. A. Becker, B. A. Brown, and S. Raman, Phys. Rev. C **34**, 1031 (1986).
[25] S. Raman, R. F. Carlton, J. C. Wells, E. T. Jurney, and J. E. Lynn, Phys. Rev. C **32**, 18 (1985).
[26] R. M. Freeman, R. Faerber, M. Toulemonde, and A. Gallmann, Nucl. Phys. A **197**, 529 (1972).
[27] A. Guichard, H. Nann, and B. D. Wildenthal, Phys. Rev. C **12**, 1109 (1975).
[28] Th. W. Van Der Mark and L. K. Ter Veld, Nucl. Phys. A **181**, 196 (1972).
[29] B. Fornal *et al.*, Phys. Rev. C **49**, 2413 (1994).
[30] N. Nica, J. Cameron, and B. Singh, Nucl. Data Sheets **113**, 1 (2012), and references therein.
[31] C. Rossi Alvarez, Nucl. Phys. News **3**, 10 (1993).
[32] M. Piiparinen *et al.*, Nucl. Phys. A **605**, 191 (1996).
[33] W. D. Hamilton, *The Electromagnetic Interaction in Nuclear Spectroscopy* (North-Holland, Amsterdam/American Elsevier, New York, 1975), Chap. 12.
[34] P. M. Endt, At. Data Nucl. Data Tables **23**, 3 (1979).
[35] J. C. Wells and N. R. Johnson, Report No. ORNL-6689, 1991, p. 44.
[36] J. F. Ziegler, *The Stopping and Range of Ions in Matter* (Pergamon Press, New York, 1980), Vols. 3 and 5.
[37] J. F. Ziegler, J. P. Biersack, and V. Littmark, *The Stopping Power and Range of Ions in Solid* (Pergamon Press, New York, 1985), Vol. 1.
[38] L. C. Northcliffe and R. F. Schilling, Nucl. Data, Sect. A **7**, 233 (1970).
[39] S. H. Sie, D. Ward, J. S. Geiger, R. L. Graham, and H. R. Andrews, Nucl. Phys. A **291**, 443 (1977).
[40] E. Caurier and F. Nowacki, Acta Phys. Pol. B **30**, 705 (1999).
[41] A. Poves, E. Caurier, F. Nowacki, and K. Sieja, Phys. Scr. T **150**, 014030 (2012).
[42] X. Liang *et al.*, Phys. Rev. C **66**, 014302 (2002).
[43] W. A. Richter, S. Mkhize, and B. A. Brown, Phys. Rev. C **78**, 064302 (2008).